Electron-phonon coupling effects on Yb^{3+} spectra in several laser crystals

1999 J. Phys.: Condens. Matter 11 3769

(http://iopscience.iop.org/0953-8984/11/18/312)

J. Phys.: Condens. Matter **11** (1999) 3769–3778. Printed in the UK PII: S0953-8984(99)01315-6

Electron–phonon coupling effects on Yb^{3+} spectra in several laser crystals

A Lupei†, V Lupei†, C Presura†, V N Enaki‡ and A Petraru†

† Institute of Atomic Physics, PO Box R-76900, Bucharest, Romania
‡ Chisinau State University, Moldavian Republic

Received 25 January 1999

Abstract. The complex absorption spectra of Yb^{3+} in YAG, $LiNbO_3$ and YLF, three important laser crystals, are analysed in terms of electron–phonon coupling effects. The local symmetry for Yb^{3+} in these crystals is noncentrosymmetric allowing the coexistence of several electron–phonon coupling mechanisms in the formation of vibronic spectra. The shape of several Yb^{3+} absorption lines is interpreted in terms of the near resonant electron–phonon coupling theory. The computer modelling, by taking into account more phonons in the resonance region enables the assignment of crystal-field levels of the Yb^{3+} $^2F_{5/2}$ multiplet and an estimation of electron–phonon coupling strengths. The phonons involved in the near resonance processes were observed in Raman spectra too. For YAG the modelling with a phonon density with four peaks in the near resonant region is made and it gives a good description of the complex experimental pattern. In the case of Yb^{3+} in $LiNbO_3$ and YLF the use of polarization data evidences also the symmetry characteristics of the electron–phonon coupling.

1. Introduction

The recent interest in investigation of electron–phonon interaction of Yb^{3+} ($4f^{13}$) ion in various materials presents a fundamental character in connection with the elucidation of the nature of its strong coupling with the lattice phonons and a practical one due the importance of this ion as a laser active centre for $\sim$1.0 μm emission or as sensitizer for emission of other rare earth (RE^{3+}) ions. In its $4f^{13}$ configuration Yb^{3+} has only two multiplets, a $^2F_{7/2}$ ground state and a $^2F_{5/2}$ excited state that are split in local crystal fields. Though the electronic structure of this ion is simple, the optical spectra are rather complex, in connection with vibronics. The investigation of vibronics provides information on the strength of electron–phonon coupling, important also for multiphonon relaxations and phonon assistance of energy transfer phenomena involved in sensitization.

For a noncentrosymmetric local symmetry at the RE^{3+} ions the optical transitions are dominated by electric-dipole-induced transitions. Three possible contributions to the intensity of vibronic sidebands were discussed in the literature [1]: Franck–Condon and Hertzberg–Teller mechanisms that are connected to the diagonal and nondiagonal respectively matrix elements of even electronic part of the linear vibronic coupling operator, and the Van Vleck mechanism that contains the odd part of the vibronic operator. The appearance of phonon replicas is a direct proof of the Franck–Condon mechanism, while the near resonant electron–phonon effects could be connected with the Hertzberg–Teller mechanism.

Since the Stark splittings of the RE^{3+} ions in crystals are of the order of the lattice optical phonons, besides the usual effects of electron–phonon coupling, near resonant processes could

0953-8984/99/183769+10$19.50

appear: if the vibronic states connected with one electronic level are in near resonance with another electronic nondegenerate level, the electron–phonon interactions can couple these states and creates new vibronic states. This induces modification of the optical spectral lines (broadening, asymmetries, splittings) or temperature-dependent effects on zero-phonon lines. Due to these effects the assignment of the crystal-field electronic levels is sometimes ambiguous. The attempts to obtain reliable experimental electronic energy level diagrams for some RE^{3+} ions have revealed a series of anomalies in the spectra. At least two conditions are necessary to have intense near resonant effects: rather strong electron–phonon coupling and sharp peaks in the phonon density in the resonance region. We quote some of the relevant reported experimental data on resonance effects in ionic compounds [2–10] that refer especially to Ce^{3+} ($4f^1$), Pr^{3+} ($4f^2$), Tm^{3+} ($4f^{12}$), Yb^{3+} ($4f^{13}$) and Tm^{2+} ($4f^{13}$), i.e. RE^{3+} ions at the beginning and the end of lanthanide series that present rather strong electron–phonon interaction, as discussed recently [11, 12].

The paper discusses some aspects of the electron–phonon coupling observed in optical spectra of Yb^{3+} doped in several important laser crystals such as $Y_3Al_5O_{12}$ (YAG), $LiNbO_3$ and $LiYF_4$ (YLF). The shielding of 4f electrons by 5s and 5p, which shows a gradual decrease along the lanthanide series and has a minimum for Yb^{3+} (0.6), was considered as the main factor for surprisingly large electron–phonon coupling strength [12] of this ion. The local symmetry at the Yb^{3+} ion in all these crystals is noncentrosymmetric. Attention is paid mainly to near resonant effects. Data are analysed with a theoretical treatment of near resonant electron–phonon effects that extends the previous approaches [13–18] to describe various effects such as the lineshape in the case of near resonant coupling with more phonons or the one-phonon contribution to temperature effects of zero-phonon lines.

2. Experiment

The crystals under study were grown by pulling from the melt by the Czochralski method. The Yb^{3+} concentration in the melt was ∼5 at.% in YAG, 0.2 at.% in stoichiometric $LiNbO_3$ and 20 at.% in YLF. The transmission measurements under lamp pumping have been measured with a set-up including a computer-controlled 1 m GDM monochromator, an S_1 photomultiplier and a multichannel MCS analyser.

3. Theoretical background

The lineshape of a transition from an initial pure electronic isolated state $|i\rangle$ to a final state $|f\rangle$, that is separated by another electronic level r with $\Delta_{f,r} = E_f - E_r > 0$ such that $\Delta_{f,r}$ is nearly equal to ω_k, a peak in the phonon spectrum, is calculated taking into account the near resonant electron–phonon interaction. The electron–phonon interaction Hamiltonian is considered in the linear approximation $H_{el} = \sum_k V_k Q_k$, with Q_k a normal vibration mode k and V_k the electron–phonon coupling operator. The lineshape for a transition induced by light of frequency Ω takes the form [15]

$$F(\Omega) = \frac{1}{\pi} \sum_f |\langle i|d|f\rangle|^2 \frac{\gamma + \Gamma_f(\Omega)}{[\Omega - \Omega_{f,i} - \Sigma_f(\Omega)]^2 + [\gamma + \Gamma_f(\Omega)]^2} \tag{1}$$

where $|\langle i|d|f\rangle|^2$ is proportional to the intensity of the zero-phonon line in the absence of near resonant electron–phonon interaction, d is the effective operator of the optical transition, γ is the electronic linewidth, $\Omega_{f,i}$ is the electronic transition energy in the absence of electron–phonon coupling and the analytical expressions for $\Sigma(\Omega)$ and $\Gamma(\Omega)$ for the resonant case are

obtained [13–15] by considering an effective phonon density $\rho(\omega)$.

$$\Gamma(\Omega) = \frac{\pi}{h^2}\sum_r \int_0^\infty A_r(\omega)\rho(\omega)\{[n(\omega)+1]\delta(\Omega - \Omega_{f,i} + \Delta_{f,r} - \omega) + n(\omega)\delta(\Omega - \Omega_{f,i} + \Delta_{f,r} + \omega)\}\,\mathrm{d}\omega \quad (2)$$

$$\Sigma(\Omega) = \frac{1}{h^2}\sum_r P\int_0^\infty A_r(\omega)\rho(\omega)\left[\frac{n(\omega)+1}{\Omega - \Omega_{f,i} + \Delta_{f,r} - \omega} + \frac{n(\omega)}{\Omega - \Omega_{f,i} + \Delta_{f,r} + \omega}\right]\mathrm{d}\omega. \quad (3)$$

The matrix elements of the electron–phonon coupling operator are contained in $A_r \sim |\langle f|V_k|r\rangle|^2$ that could be estimated in various approximations, or enter as adjustable experimental parameters, $n(\omega)$ is the phonon occupation number and P signifies the principal value of the integral. The temperature dependence of the linewidth and the position of a level f is obtained in the one-phonon approximation from Γ (2) and Γ (3) with $\Omega = \Omega_{fi}$.

To account for the coupling with more phonons in the resonance region, the problem must be solved numerically. For this purpose the relations (1)–(3) are used by considering the phonon density $\rho(\omega)$ in the resonance region as a weighted sum of Lorentz peaks:

$$\rho(\omega) = \sum_i a_i \nu_i(\omega) \text{ with } \nu_i(\omega) = \frac{1}{\pi}\frac{\alpha_i}{(\omega - \omega_i)^2 + \alpha_i^2} \quad (4)$$

where a_i is the contribution of phonon i and α_i is the halfwidth of the phonon peak.

4. Results and discussion

4.1. Yb^{3+} in YAG

Yb^{3+} replaces in YAG the Y^{3+} ions in dodecahedral sites of D_2 local symmetry and its two multiplets, $^2F_{7/2}$ ground and $^2F_{5/2}$ excited state, are split into four and respectively three Stark doublets. Figure 1(a) presents the absorption spectrum at 10 K, corresponding to $^2F_{7/2}(1) \rightarrow {}^2F_{5/2}$ transitions of Yb^{3+} (5 at.%) in YAG. The measured complex spectra were connected to electron–phonon interaction effects, but the assignments of the electronic Stark levels were contradictory [19–25], especially as concerns the $^2F_{5/2}$ multiplet. While the $^2F_{7/2}(1) \rightarrow {}^2F_{5/2}(1)$ transition was identified at 10 327 cm^{-1} (line A), the main problem was to assign the other two 'pure' electronic lines from the three main features (B, B′, C), at 10 624, 10 679 and 10 912 cm^{-1}, respectively (figure 1(a)). If in [20] and [21] the choice was B, B′, the crystal field calculations [23, 24] suggest the presence of the third electronic level in the C region, but the ambiguity in the assignment of B, B′ lines still remained.

In our previous reports [26, 27] we have proposed a simplified model to assign the electronic levels of Yb^{3+} in YAG based on near resonant effects. Thus, B and B′ lines are considered as the split components of the second Stark level E_2 of $^2F_{5/2}$ due to resonant coupling with a phonon of 326 cm^{-1}, while C and C′ lines correspond to the splitting of the third Stark level E_3, the phonon involved being of 600 cm^{-1}. Although this model describes the main features of the spectra, the details observed for lines B and B′ were neglected.

To account for the complex observed structure in the B, B′ region of the absorption spectrum at 10 K, the phonon density $\rho(\omega)$ in the resonance region is taken as a weighted sum of Lorentz peaks and a computer fitting of the spectra is performed. The result of the numerical modelling of absorption by using equations (1)–(3) and taking into account only near resonant coupling with four phonons in the B, B′ and one phonon in C, C′ region is presented in figure 1(b), where the estimated positions of crystal field levels E_i of $^2F_{5/2}$ are marked and the best fit parameters are given in table 1. This table contains the position of split electronic level E_i as determined from fitting, the width of the electronic line γ, the resonant phonon energy ω,

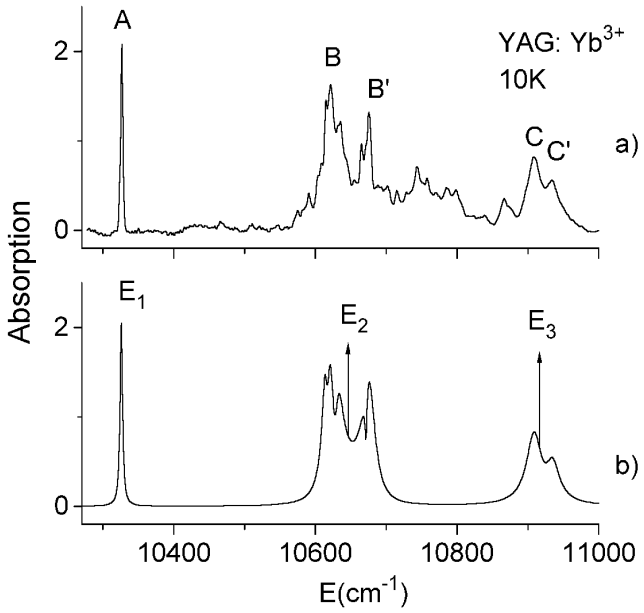

Figure 1. (a) Absorption spectrum of Yb^{3+} (5 at.%) in YAG at 10 K $^2F_{7/2}(1) \rightarrow {}^2F_{5/2}$ transition. (b) Theoretical modelling; E_i are the Stark levels of $^2F_{5/2}$.

Table 1. Parameters used for modelling the lineshapes of several Yb^{3+} absorptions in near resonant coupling.

Crystal	Yb^{3+} level E_i (cm^{-1})	Yb^{3+} level linewidth γ (cm^{-1})	Phonon energy ω (cm^{-1})	Phonon linewidth	Coupling $A(\omega)^*a$	Crystal phonon peaks (Raman)
			289	3	20	290
			300	4	60	305
YAG	E_2—10 646	5	327	18	700	325
			344	1	20	340
	E_3—10 914	14	599	10	140	600
$LiNbO_3$	E_2—10 462	50	232	5	90	232
			270	8	150	270
YLF	E_3—10 559	10	272	5	50	273

phonon halfwidth α_i, coupling parameter $A(\omega)^*a$ and vibrational data obtained for the given crystal by Raman or i.r. One can see (table 1) that for Yb^{3+} in YAG the main contribution to the splitting in the B, B′ region comes from the coupling with the phonon 327 cm^{-1}, as expected, while the details of the spectrum are given by the phonons located at: 289 cm^{-1}, 300 cm^{-1} and 344 cm^{-1}. Phonons with frequencies close to these have been observed in the Raman spectra or phonon sidebands [28, 29]. The electronic crystal-field energy levels in YAG obtained from this fitting are 10 327, 10 646, 10 914 cm^{-1} as illustrated in figure 1(b). Since in D_2 the Stark components are Γ_5 Kramers doublets, group symmetry tables [33] show that no symmetry restrictions could be imposed on the phonon coupling. Most of the other vibronic peaks observed in the absorption spectrum of Yb^{3+}:YAG (figure 1(a)), which are not involved in resonance, could be associated with line A [22, 26].

A red thermal shift of line A is observed. In order to describe the experimental temperature dependences of linewidth and the shift of the zero phonon line A the contribution of initial and final levels involved in the transition should be considered. Since up to 300 K the population of the second Stark level of the ground multiplet $^2F_{7/2}$, situated at 565 cm^{-1}, can be neglected, one could consider only the one-phonon processes involved in the upper level E_1 of the $^2F_{5/2}$ Yb^{3+} multiplet, i.e. the contribution coming from B, B′ near resonance. If the broadening can be rather well described with the coupling parameters from table 1, the thermal shifts are systematically smaller, suggesting the contribution of other processes too.

4.2. Yb^{3+} in $LiNbO_3$

Since $LiNbO_3$ is a uniaxial crystal of space group C_{3v}^6 the absorption measurements, unlike the previous reported ones [30], were performed in two polarizations. The previous reports on RE^{3+} ions in $LiNbO_3$ led to the conclusion that they can replace Li^+ and the charge compensation is nonlocal [30]. Several slightly different RE^{3+} centres were observed [31, 32] in the case of Nd^{3+}, Er^{3+}, Pr^{3+}. The local symmetry at the RE^{3+} ion is C_{3v} or C_3. Since the octahedral sites in $LiNbO_3$ present a small departure from C_{3v}, one could consider this symmetry as a good approximation in the analysis of Yb^{3+} spectra.

The $\sigma(E \perp C_3)$ and $\pi(E \parallel C_3)$ absorption spectra at 10 K for a sample of Yb^{3+} (0.2 at.%): $LiNbO_3$ are presented in figure 2. The σ spectrum (figure 2(a)) is complex, but shows three clear features A, B and C, while in the π spectrum only the A line has significant intensity, B is missing and C has a very low intensity (figure 2(b)). For low concentration samples, no evidence of more Yb^{3+} centres in line A is given by the resolution of our experiment. A blue shift of this line A with increasing temperature is observed. The anomalous shape of line B and the other features of the σ spectrum will be analysed in terms of electron–phonon coupling.

For C_{3v} symmetry the two Yb^{3+} multiplets $^2F_{7/2}$ and $^2F_{5/2}$ are split into Stark doublets

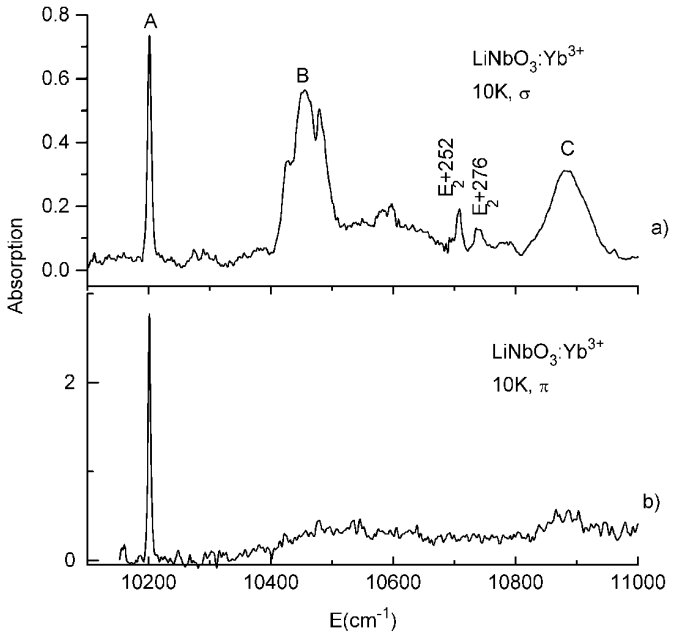

Figure 2. The polarized absorption spectra of Yb^{3+} in $LiNbO_3$ at 10 K.

characterized by the irreducible representations Γ_4 and $(\Gamma_5 + \Gamma_6)$: $^2F_{7/2} \rightarrow 3\Gamma_4 + (\Gamma_5 + \Gamma_6)$ and $^2F_{5/2} \rightarrow 2\Gamma_4 + (\Gamma_5 + \Gamma_6)$, respectively [33]. The selection rules for the electric–dipole transitions in this case are $\Gamma_4 \otimes \Gamma_4 = \Gamma_1 + \Gamma_2 + \Gamma_3$, $\Gamma_4 \otimes (\Gamma_5, \Gamma_6) = \Gamma_3$, $\Gamma_5 \otimes \Gamma_5 = \Gamma_1$, $\Gamma_6 \otimes \Gamma_6 = \Gamma_1$ and Γ_1 transforms as z, Γ_3 as $(x - iy)$ and $(x + iy)$ and Γ_2 as S_z. Group theory together with polarization spectra can be used in the attempt to assign the irreducible representations to Stark levels. Since the local symmetry is a trigonally distorted octahedron one could start from the splitting of J multiplets in octahedral symmetry. The cubic octahedral field of O_h symmetry splits the upper $^2F_{5/2}$ multiplet into two levels whose wave functions transform as Γ_7^- and Γ_8^-, the last level lying at lower energy. The ground multiplet $^2F_{7/2}$ is split into Γ_6^-, Γ_7^- and Γ_8^-, with Γ_6^- the lowest Stark level and Γ_8^- in the middle. In C_{3v}, the doublets Γ_6^-, Γ_7^- correspond to Γ_4, while Γ_8^- is split into the doublets Γ_4 and $(\Gamma_5 + \Gamma_6)$. The order of Stark doublets obtained from Γ_8^- cannot be distinguished without a crystal-field calculation. If the axial symmetry leaves Γ_4 as the ground level of the $^2F_{7/2}$ multiplet, the polarization results (lines A and C are observed in π polarization and lines A, B and C in the σ spectrum) could be explained if one assumes that the three Stark levels of the excited multiplet $^2F_{5/2}$ are E_1—Γ_4, E_2—$(\Gamma_5 + \Gamma_6)$ and E_3—Γ_4. The splittings of the ground state $^2F_{7/2}$ 0, (260, 437), 763 cm^{-1} [30] and excited state $^2F_{5/2}$ (10 201.5, 10 462), 10 882 cm^{-1} (this work), where the levels associated with the parent electronic state Γ_8^- are in parentheses, suggest a dominance of the octahedral crystal field over the axial one. If the data are analysed in terms of C_3 local symmetry the polarization characteristics of the spectra are not changed. This can be easily observed if the compatibility representation tables of C_{3v} and C_3 and selection rules for electric dipole transitions are used [33]. For the sake of simplicity the vibronic data are analysed in terms of C_{3v} symmetry.

The complex σ spectrum of Yb^{3+} in $LiNbO_3$ could be explained in terms of vibronic transitions and near resonant effects. The space group character table for C_{3v}^6 shows that the i.r. and Raman active phonons for $k = 0$ are reduced [33, 34] in local symmetry C_{3v} of the RE^{3+} ion to $A_1(\Gamma_1)$ and $E(\Gamma_3)$ modes, while $A_2(\Gamma_2)$ modes are inactive Raman or i.r. To explain the shape of the spectrum in the B region we assume a near resonant electron–phonon coupling between E_1 and E_2 levels. The symmetry selection rules for resonant coupling are contained in the matrix elements of the electron–phonon coupling operator $A_r \sim |\langle f|V_k|r\rangle|^2$, where $|f\rangle$ and $|r\rangle$ are electronic wavefunctions. The symmetry characteristics of E_1 and E_2 suggest that a coupling between them is possible with $E(\Gamma_3)$ phonons since $\Gamma_4 \otimes (\Gamma_5, \Gamma_6) = \Gamma_3$. More $E(\Gamma_3)$ type phonons with energies close to $E_2 - E_1$ were observed in Raman spectra [35], but the coupling only with two, 232 and 270 cm^{-1}, is considered. A modelling of the σ spectrum in the B region is presented in figure 3(b) and the fitting parameters are given in table 1. We should mention that the rather large width of the central peak could be connected either with the coupling with other phonons [35] or with the presence of different Yb^{3+} centres. The presence of several structural Yb^{3+} centres is possible, but one should expect to observe it in line A (fairly narrow) too; however we did not detect any structure for this line in the limits of the resolution of our experiment. Taking into account the compatibility tables between C_{3v} and C_3 representations [33], A_1, $A_2 \rightarrow A$ and $E \rightarrow E$ and the fact that A_2 modes are inactive, this analysis is valid in C_3 symmetry too.

To explain the other phonon sidebands we have compared the vibronics with Raman or infrared data [34, 35] of $LiNbO_3$ The comparison of π and σ spectra suggests that the phonon sidebands observed in the σ spectrum must be connected with the E_2 level. The main two vibronics observed in the σ spectrum (figure 2(a)) are at 247 and 276 cm^{-1} from E_2 (as determined from resonance data) while the Raman data [35] at 10 K show two A_1 phonons at $\sim$250 and $\sim$270 cm^{-1}. Phonons of similar energies 248 and 274 cm^{-1} were observed in i.r. spectra too [34].

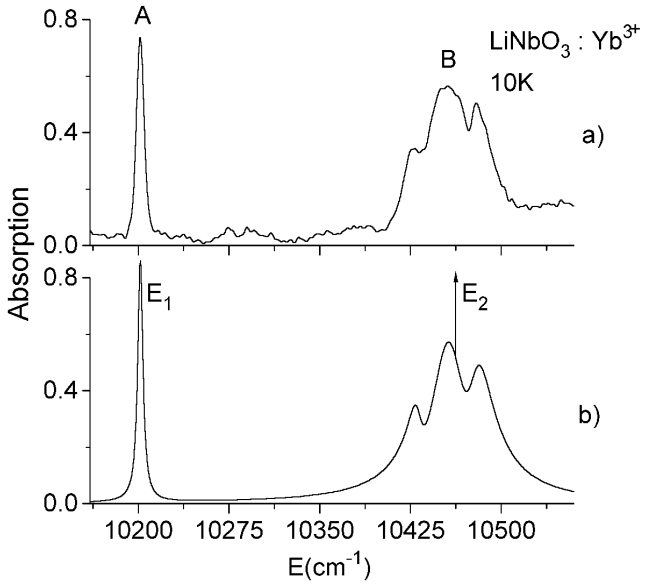

Figure 3. (a) Part of the absorption spectrum of Yb^{3+} in $LiNbO_3$ at 10 K and (b) Theoretical modelling of the lineshape.

The blue thermal shift of line A in the case of Yb^{3+} in $LiNbO_3$ imposes the consideration of the one–phonon contribution of the lower level of the $^2F_{7/2}$ multiplet too, since its Stark components are in the range of the phonon spectrum and near resonance effects are possible. The one-phonon contributions [14] can have different signs and an accurate estimation is difficult. Our estimations show, however, that the blue shift must come from a lower level contribution.

4.3. Yb^{3+}:YLF

The σ and π absorption spectra of Yb^{3+} in YLF are presented in figures 4(a), (b). Yb^{3+} replace in YLF Y^{3+} sites of S_4 local symmetry. For S_4 symmetry the free ion multiplets are split as follows [33]: $^2F_{7/2} \rightarrow 2(\Gamma_5 + \Gamma_6) + 2(\Gamma_7 + \Gamma_8)$ and $^2F_{5/2} \rightarrow 2(\Gamma_5 + \Gamma_6) + (\Gamma_7 + \Gamma_8)$, respectively. The selection rules for electric–dipole transitions can be deduced from the direct products: $\Gamma_{5,6} \otimes \Gamma_{5,6} \rightarrow 2\Gamma_1 + (\Gamma_4 + \Gamma_3)$, $\Gamma_{5,6} \otimes \Gamma_{7,8} \rightarrow 2\Gamma_2 + (\Gamma_3 + \Gamma_4)$, and $\Gamma_{7,8} \otimes \Gamma_{7,8} \rightarrow 2\Gamma_1 + (\Gamma_3 + \Gamma_4)$, knowing that the representation Γ_3 transforms as $i(x - iy)$, Γ_4 as $-i(x + iy)$ and Γ_2 as z. In order to explain the polarization spectra, the following assignment is proposed: the ground Stark level of $^2F_{7/2}$ is $\Gamma_{5,6}$, as given by EPR data [37], and the order of excited Stark levels of $^2F_{5/2}$ is $\Gamma_{5,6}$, $\Gamma_{7,8}$, $\Gamma_{5,6}$. This would give a B line polarized σ and π and A, B and C lines polarized σ. The presence of the A line in the π spectrum could be determined by depolarization in measurements.

From the shape of the lines and the i.r. and Raman spectra [38, 39] one could consider that the shape of the line C, observed in the σ spectrum, involves a resonance process between E_1 and E_3 Stark levels of an excited multiplet with a Raman phonon [39] of 273 cm^{-1}, having A (Γ_1) symmetry. Indeed the symmetry characteristics of $E_1(\Gamma_{5,6})$ and $E_2(\Gamma_{5,6})$ suggest that a nonvanishing coupling given by $A_r \sim |\langle f|V_k|r\rangle|^2$ is possible with phonons of Γ_1 (A) or Γ_4, Γ_3 (E) type. The analysis of the shape with resonance relations (1)–(3) gives the electronic level

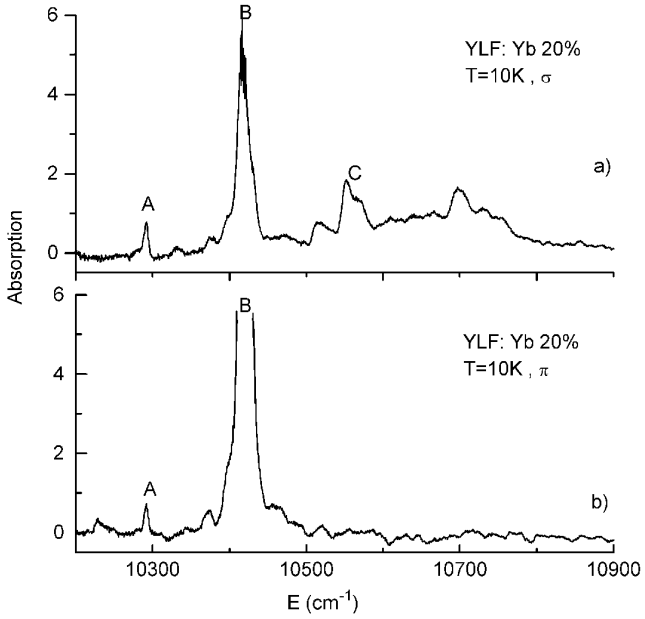

Figure 4. The polarized absorption spectra of Yb^{3+} (20 at.%) in YLF at 10 K.

E_3 at 10 559 cm^{-1} and the involved phonon energy is 272 cm^{-1} (table 1). Thus, the electronic Stark levels of $^2F_{5/2}$ multiplet are 10 290, 10 418, 10 559 cm^{-1}. Since line C is missing in the π polarization along with other features at higher energies one can assume that these are vibronics connected with the E_3 level. The assignment of these lines and other vibronics observed in σ spectrum is given in figure 5, where the spectrum is normalized to line A. These phonons have been observed in Raman [39] (182—B, 273—A(cm^{-1})) or i.r. [38] (143—E, 173—A, 195—A, 224—A(cm^{-1})) spectra. The most intense phonon sidebands observed in the spectra (figure 5) could be connected with i.r. phonons, suggesting the predominance of the Van Vleck mechanism [1].

5. Conclusions

This paper analyses the complex low temperature Yb^{3+} absorption spectra in several laser crystals:, $Y_3Al_5O_{12}$, $LiNbO_3$ and $LiYF_4$. The common features of these crystals are the noncentrosymmetric local symmetry at the RE^{3+} ion that allows more mechanisms for vibronic intensity and the existence of rather sharp peaks in the lattice phonon density. The Stark structure of Yb^{3+} overlaps with phonon spectra and could determine near resonant electron–phonon effects, the creation of mixed electron–phonon states, that can determine the splittings of electronic levels and redistribution of intensities.

The experimental data are analysed by using the lattice phonons given by Raman and i.r. measurements or from vibronic data reported for other RE^{3+} ions. Since Yb^{3+} in YAG and YLF replaces Y^{3+}, with similar ionic radius, the vibrational properties of the surroundings are not expected to be changed by substitution and the vibronic energies are almost identical with peaks in the host lattice phonon spectrum. In the case of $LiNbO_3$, though Yb^{3+} substitute for Li^+, the vibronic data are also well described by using the phonon energies determined at low temperatures by Raman or i.r. data.

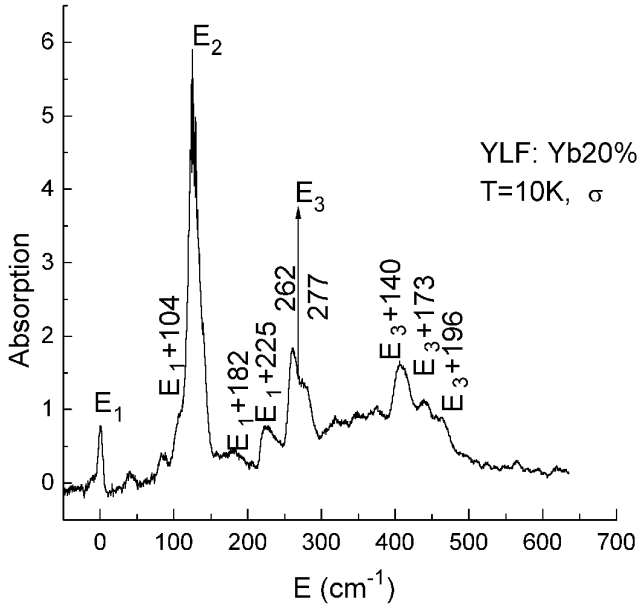

Figure 5. The assignment of phonon sidebands for the σ absorption spectrum of Yb^{3+} in YLF.

The shape of several absorption lines is interpreted on the basis of a theoretical treatment of the near resonant electron–phonon coupling between two Stark electronic levels, in near resonance with more phonon peaks. The phonons involved in the near resonance processes have been observed in Raman spectra (table 1). As the theory and fittings show, the position of electronic levels estimated in the near resonance cases do not coincide with the maxima observed in the structure of absorption lines. In this study a simulation of the complex low temperature absorption spectra of Yb^{3+} in YAG was performed. In the case of Yb^{3+} in $LiNbO_3$ and YLF the polarization data and group theory arguments are used in an attempt to assign irreducible representations to the Stark levels and the symmetry characteristics of the electron–phonon coupling. Other vibronic lines are also assigned.

In conclusion, for all these three important laser crystals the electron–phonon interactions could account for the complex Yb^{3+} optical spectra and for several regions the spectra are modelled on the basis of the near resonant coupling theory that allows the estimation of the positions of the crystal-field Stark levels, that cannot be obtained directly from measurements. The electron–phonon coupling strength estimations show a tendency of increasing from fluorides to oxides.

Note added in proof. One of the referees has drawn our attention to a paper dealing with polarized optical spectra of Yb^{3+} in $LiNbO_3$ published very recently, 1999, in *J. Phys.: Condens. Matter* **11** 311, where the electronic structure is analysed in terms of C_3 symmetry. Our analysis is compatible with the results of this paper, with slight differences in the values of electronic level position.

References

[1] Ovsyankin V V 1987 *Spectroscopy of Solids Containing Rare Earth Ions* ed A A Kaplyanskii and R M Macfarlane (Elsevier) p 343
[2] Schaack G 1977 *Z. Phys.* B **26** 49
[3] Dahl M and Schaack G 1986 *Phys. Rev. Lett.* **56** 232

[4] Gerlinger H and Schaack G 1986 *Phys. Rev.* B **33** 7438
[5] Caro Moune P O K, Antic-Fidancev E and Lemaitre-Blaise M 1985 *J. Less-Common Met.* **112** 153
[6] Lupei A and Lupei V 1997 *J. Phys.: Condens. Matter* **9** 2807
[7] Perlin Yu E, Kaminskii A A, Enaki V N and Vileghanin D N 1979 *Pis. Zh. Eksp. Teol. Fiz.* **30** 426 (in Russian)
[8] Becker P C, Williams G M, Edelstein N M, Koningstein J A, Boatner L A and Abraham M M 1992 *Phys. Rev.* B **45** 5027
[9] DeLoach L D, Payne S A, Kway W L, Tassano J B, Dixit S N and Krupke W F 1994 *J. Lumin.* **62** 85
[10] Ignatiev I and Ovsyankin V 1997 *J. Lumin.* **72–4** 679
[11] Ellens A, Andreas H ter Heerdt M L H, Wegh R T, Meijerink A and Blasse G 1997 *Phys. Rev.* B **55** 180
[12] Ellens A, Andreas H, Meijerink A and Blasse G 1997 *Phys. Rev.* B **55** 173
[13] Perlin Yu E and Tsukerblat B S 1974 *Electron–Phonon Interaction in Optical Spectra of Paramagnetic Impurities* (Chisinau: Stiinta) (in Russian)
[14] Perlin Yu E, Kaminskii A A, Klokishner S I, Enaki V N, Bogomolova G A and Vileghanin D N 1977 *Phys. Status Solidi* a **40** 643
[15] Perlin Yu E and Enaki V N 1981 *Physical Processes in Semiconductors* (Chisinau: Stiinta) (in Russian)
[16] Enaki V N 1988 *Nonequilibrium Processes in Multicomponent Crystals* vol 36 (Chisinau: Stiinta) (in Russian)
[17] Enaki V N, Lupei A, Lupei V, Presura C and Ciobu V E 1995 *Proc. SPIE* **3405** 570
[18] Malta O L *J. Phys. Chem. Sol.* **56** 1053
[19] Wood D L 1963 *J. Chem. Phys.* **39** 1671
[20] Buchanan R A, Wickersheim K A, Pearson J J and Herrmann G F 1967 *Phys. Rev.* **159** 245
[21] Pearson J J, Herrmann G F, Wickersheim K A and Buchanan R A 1967 *Phys. Rev.* **159** 251
[22] Bogomolova G A, Vylegzhanian D N and Kaminskii A A 1976 *Sov. Phys.–JETP* **42** 440
[23] Bogomolova G A, Bumagina L A, Kaminskii A A and Malkin B Z 1977 *Sov. Solid State Phys.* **19** 1439
[24] Nekvasil V 1982 *Phys. Status Solidi* b **109** 67
[25] Kaminskii A A 1981 *Laser Crystals* (Berlin: Springer) p 146
[26] Lupei A, Enaki V N, Lupei V, Presura C and Petraru A 1998 *J. Alloys Compounds* **275/276** 196
[27] Lupei A, Lupei V, Enaki V N, Presura C and Petraru A 1998 *Spectrochim. Acta* A at press
[28] Markushev V M, Tsaryuk V I and Zolin V F 1985 *Opt. Spectrosc.* **58** 583 (in Russian)
[29] Jekov V I, Murina T M, Polivanov Yu N, Popova M N and Prohorov A M 1985 *Sov. Solid State Phys.* **25** 1510 (in Russian)
[30] Burns G, O'Kane D F and Title R S 1968 *Phys. Rev.* **167** 314
[31] Lorenzo A, Jaffrezic H, Roux B, Boulon G, Bausa L E and Garcia Sole J 1995 *Phys. Rev.* B **52** 6278
[32] Munos-Santiuste J E, Lorenzo A, Bausa L E and Garcia-Sole J 1998 *J. Phys.: Condens. Matter* **10** 7653
[33] Koster G F, Dimmock J O, Wheeler R G and Statz H 1963 *Properties of the Thirty-two Point Groups* (Cambridge, MA: MIT Press)
[34] Barker A S and Loudon R Jr 1967 *Phys. Rev.* **158** 433
[35] Johnston D J and Kaminov I P 1968 *Phys. Rev.* **168** 1045
[36] Morrison C A and Leavitt R P 1982 *Handbook on Physics and Chemistry of Rare Earths* vol 5, ed K A Gschneidner Jr and L Eyring (Amsterdam: North-Holland)
[37] Sattler Y P and Namerich J 1971 *Phys. Rev.* B **4** 1
[38] Miller S A, Rast H E and Caspers H H 1970 *J. Chem. Phys.* **52** 4172
[39] Schltheiss E, Scharmann A and Schwabe D 1986 *Phys. Status Solidi* b **138** 465